J Neurophysiol 94: 3357–3367, 2005.
First published July 6, 2005; doi:10.1152/jn.00076.2005.

Two Populations of Layer V Pyramidal Cells of the Mouse Neocortex: Development and Sensitivity to Anesthetics

Elodie Christophe,[1] Nathalie Doerflinger,[1] Daniel J. Lavery,[2] Zoltán Molnár,[3] Serge Charpak,[1] and Etienne Audinat[1]

[1]*Laboratoire de Neurophysiologie, Institut National de la Santé et de la Recherche Médicale, Centre National de la Recherche Scientifique, Ecole Supérieure de Physique et Chimie Industrielles, Paris, France;* [2]*Purdue Pharma L.P., Cranbury, New Jersey; and* [3]*Department of Human Anatomy and Genetics, University of Oxford, South Parks Road, United Kingdom*

Submitted 21 January 2005; accepted in final form 29 June 2005

Christophe, Elodie, Nathalie Doerflinger, Daniel J. Lavery, Zoltán Molnár, Serge Charpak, and Etienne Audinat. Two populations of layer V pyramidal cells of the mouse neocortex: development and sensitivity to anesthetics. *J Neurophysiol* 94: 3357–3367, 2005. First published July 6, 2005; doi:10.1152/jn.00076.2005. Previous studies have shown that layer V pyramidal neurons projecting either to subcortical structures or the contralateral cortex undergo different morphological and electrophysiological patterns of development during the first three postnatal weeks. To isolate the determinants of this differential maturation, we analyzed the gene expression and intrinsic membrane properties of layer V pyramidal neurons projecting either to the superior colliculus (SC cells) or the contralateral cortex (CC cells) by combining whole cell recordings and single-cell RT-PCR in acute slices prepared from postnatal day (P) 5–7 or P21–30 old mice. Among the 24 genes tested, the calcium channel subunits α1B and α1C, the protease Nexin 1, and the calcium-binding protein calbindin were differentially expressed in adult SC and CC cells and the potassium channel subunit Kv4.3 was expressed preferentially in CC cells at both stages of development. Intrinsic membrane properties, including input resistance, amplitude of the hyperpolarization-activated current, and action potential threshold, differed quantitatively between the two populations as early as from the first postnatal week and persisted throughout adulthood. However, the two cell types had similar regular action potential firing behaviors at all developmental stages. Surprisingly, when we increased the duration of anesthesia with ketamine–xylazine or pentobarbital before decapitation, a proportion of mature SC cells, but not CC cells, fired bursts of action potentials. Together these results indicate that the two populations of layer V pyramidal neurons already start to differ during the first postnatal week and exhibit different firing capabilities after anesthesia.

INTRODUCTION

Layer V pyramidal neurons in the adult rodent cortex fall into two major classes according to their axonal projection sites, which can be either the subcortical structures (e.g., spinal cord, superior colliculus, basal pons) or the contralateral cortex (Hallman et al. 1988; Ivy and Killackey 1982; Kasper et al. 1994a; Wise and Jones 1976). In rat, axons of these two classes grow toward their appropriate targets at embryonic day (E) 18 and invade them between postnatal day (P) 0 and P3 (Kasper et al. 1994c; Koester and O'Leary 1992). Throughout embryonic and postnatal life, an individual neuron does not send branching axons to both cortical and subcortical targets (Hallman et al. 1988; Koester and O'Leary 1992). Early specification of axon targeting indicates that neurons of the two classes have differentiated from each other before birth. However until P5, they retain identical somato-dendritic morphologies; in particular they all have an apical dendrite reaching layer I (Kasper et al. 1994c). Between P5 and P7, most cortico-cortical–projecting neurons (CC-projecting neurons) retract their apical tuft from layer I to layer II/III and IV. In contrast, pyramidal cells projecting to subcortical regions maintain their apical tuft in layer I throughout postnatal life (Hallman et al. 1988; Kasper et al. 1994c; Koester and O'Leary 1992).

There are some markers—Otx1, ER81, and medium-sized neurofilaments (N200, FNP-7, SMI-32)—that are preferentially expressed in the subcortically projecting, but not in the callosally projecting, pyramidal cell population (Hevner et al., 2004; Voelker et al. 2004; Weimann et al. 1999), although their significance in differentiation is not fully understood. Electrophysiological differences between these two neuronal classes have also been observed. In the neocortex of adult rodents, subcortically projecting cells fire bursts of action potentials and have a lower input resistance and a smaller membrane time constant than CC neurons, which fire action potentials more regularly (Franceschetti et al. 1993; Kasper et al. 1994a; Larkman and Mason 1990; Mason and Larkman 1990). The bursting behavior of subcortically projecting neurons, in particular the pyramidal neurons in the visual cortex projecting to the superior colliculus (SC-projecting neurons), occurred only after the second postnatal week. Before this stage they have a regular firing pattern similar to that of CC-projecting neurons (Kasper et al. 1994b,c).

Thus the maturation of layer V pyramidal cells seems to be characterized by three major steps: an embryonic specification of their axonal projection territories; an early postnatal (P5–7) differentiation of the apical dendrites (i.e., the retraction or the maintenance of the tuft in layer I); and finally a later functional differentiation (P15–21), which consists in the acquisition or not of a bursting behavior that is not apparent before the third postnatal week (Kasper et al. 1994b). Beside the sequential specification of these three parameters, layer V pyramidal cells express other characteristics that also evolve gradually during the first three postnatal weeks. This is the case for the resting membrane potential, the input resistance, and the action potential duration and amplitude (Franceschetti et al. 1998; Kasper

Address for reprint requests and other correspondence: E. Audinat, Neurophysiology and New Microscopies Laboratory, INSERM U603, CNRS FRE 2500, Université Paris Descartes, 45 Rue des StPères, 75006 Paris, France (E-mail: etienne.audinat@univ-paris5.fr).

The costs of publication of this article were defrayed in part by the payment of page charges. The article must therefore be hereby marked "*advertisement*" in accordance with 18 U.S.C. Section 1734 solely to indicate this fact.

et al. 1994b; Mason and Larkman 1990; Zhang 2004; Zhu 2000) that mature with a time constant of 5 to 6 days to reach adult values at the beginning of the fourth postnatal week (Zhang 2004).

In the present study we compared the biochemical and electrophysiological properties of identified CC- and SC-projecting pyramidal neurons at the beginning and at the end of their postnatal maturation. We analyzed in vitro the expression of putative cell–type specific molecular markers and selected membrane channel mRNAs, as well as the intrinsic membrane properties of layer V projection neurons that had been retrogradely labeled from their targets, i.e., the contralateral cortex or the superior colliculus. Surprisingly, we found that CC and SC cells already differed in some of their properties during the first postnatal week and that the bursting behavior of SC- but not CC-projecting neurons varied with the duration of the anesthesia applied to the animal before decapitation.

METHODS

All protocols used followed EU and Institutional guidelines.

Injection of beads and fluorescence microscopy

To identify the two populations of layer V pyramidal cells, we pressure-injected green or red fluorescent retrobeads (approximately 3 μl; Lumafluor, Naples, FL) with a patch pipette (1–2 μm at the tip; borosilicate glass) into the left superior colliculus (green) and the right parietal associative/visual cerebral cortex (red) of P3–5 CH3 mice ($n = 82$) anesthetized on ice. Experiments were then performed in vitro on acute brain slices obtained from P5–7 ($n = 38$) and P21–30 ($n = 44$) day-old animals, i.e., 2–4 days or 2–3 wk after the injections. In preliminary experiments we verified the distribution of retrogradely labeled fluorescent neurons in layer V by fluorescence imaging, using an upright microscope (Model BX51, Olympus France) equipped with 10×/NA0.17 or 20×/NA0.95 objectives and a Quantix-EEV37 back-illuminated cooled CCD camera (Princeton Instruments, Trenton, NJ). Two Olympus filter sets (ex450–480/500DC/em >515 nm and ex510–550/570DC/em >590 nm) were used for the visualization of red and green fluorescence, respectively. Images were aligned, scaled, and analyzed in terms of cell density and cellular localization with Metamorph (Universal Imaging, Downington, PA).

Electrophysiology

Animals were anesthetized with an intraperitoneal injection of either a mixture of ketamine (65 mg/kg) and xylazine (14 mg/kg; $n = 78$) or pentobarbital (27.4 mg/kg; $n = 4$). Coronal or parasagittal sections (300 μm thick) constituting the left parietal associative cortex and the medial part of the visual cerebral cortex were prepared (Kasper et al. 1994c) using a vibroslicer (Leica, Wetzlar, Germany). Similar results were obtained with coronal or parasagittal slices, and thus results were pooled together. Slices were incubated for 10 min at 35°C and then at room temperature (20–25°C) in a recording solution containing (in mM): 126 NaCl, 2.5 KCl, 1.25 NaH_2PO_4, 2 $CaCl_2$, 1 $MgCl_2$, 20 glucose, 26 $NaHCO_3$, and 5 pyruvate and was saturated with a mixture of 95% O_2-5% CO_2 (325 mOsm/l, pH7.2).

Recordings

For the recordings, slices were transferred to a chamber perfused with extracellular solution at 2 ml per min at 33–35°C. Fluorescent pyramidal neurons from layer V were selected under visual control using an upright microscope equipped with Nomarski differential interference contrast optics and epifluorescence illumination (Leica, Wetzlar, Germany). Patch pipettes (3–5 MΩ) were pulled from borosilicate glass (Harvard Apparatus, Kent, UK) and were filled with an intracellular solution containing (in mM): 120 K-gluconate, 10 Hepes, 15 Na-gluconate, 3 $MgCl_2$, 10 phosphocreatin, 0.3 GTP, and 4 ATP-K_2 (pH = 7.2, 295 mOsm). In some experiments, the fluorescent dye Alexa Fluor 568 (20 μM; Molecular Probes) was also included in the intracellular solution. Whole cell recordings in voltage-clamp mode or fast current-clamp mode were obtained using a patch-clamp amplifier (Axopatch 200B, Axon Instruments, Foster City, CA) and all membrane potential values were corrected for a junction potential of −11 mV. In voltage-clamp recordings, the series resistance was not compensated but monitored throughout the recordings to exclude experiments that varied by more than 25%. In current-clamp recordings, the series resistance was balanced. Signals were digitized at 10–20 kHz and analyzed off-line with Pclamp 9 (Axon Instruments). Resting membrane potential, input resistance, rectification during hyperpolarizing steps, and action potential firing behavior were usually determined during the first 5 min that follow the beginning of the whole cell recording. Action potential characteristics were measured as previously described (Cauli et al. 1997, 2000). The action potential frequency adaptation was measured for discharges elicited by depolarizing 500-ms pulses by calculating the difference between the frequencies of the first and the last spike intervals divided by the frequency of the first interval of the discharge. This analysis was performed on discharges with an initial frequency between 50 and 60 Hz for P7 animals and between 150 and 200 Hz for mature mice. The input resistance was determined using voltage responses to small hyperpolarizing current pulses (usually 25 pA) inducing very little or no sag. The amplitude of the sag attributed to the hyperpolarization-activated current (Ih), which was observed for larger hyperpolarizing current pulses, was measured between the initial peak and the plateau at the end of the responses. A comparison between CC and SC cells was done for hyperpolarizing responses reaching an initial potential of −105 ± 5 mV. In voltage-clamp experiments, the amplitude of Ih currents was determined by subtracting the current at the onset of the hyperpolarizing voltage step from the current measured at the end pulse. The initial current was obtained by extrapolating at t_0 the exponential fit of the current response. All reported values are expressed as means ± SE. Between-group comparisons were performed using *t*-test and Mann–Whitney nonparametric test. All chemical products were from Sigma (St. Louis, MO).

Single-cell RT-PCR

We selected 24 genes that could potentially be expressed in different subpopulations of layer V and we studied their expression pattern by single-cell RT-multiplex PCR (RT-mPCR; Cauli et al. 1997; Ruano et al. 1995). All neurons used for this analysis were recorded in slices obtained from animals after a short anesthesia procedure (see RESULTS). After completion of the electrophysiological recordings aiming at characterizing passive and active membrane properties (see above), cytoplasm harvesting was performed usually <15 min after break-in and reverse transcription was immediately initiated as previously described (Lambolez et al. 1992). Briefly, patch pipettes were filled with 8 μl of a solution containing (in mM): 130 K-gluconate, 15 Na-gluconate, 3 $MgCl_2$, 10 Hepes, 0.2 EGTA, and 5.4 biocytin (pH 7.2, 295 mOsm). After the recording, the contents of the cell were aspirated into the pipettes and collected in a 0.2-ml test tube for reverse transcription reactions. The usual volume recovered was approximately 6.5 μl. This volume was brought to 10 μl with the following components at final concentrations as indicated: 5 μM hexamer random primers, 0.5 mM of each of the four deoxyribonucleotide triphosphates, 1.2 mM $MgCl_2$, 2 mM Tris (pH = 8), 10 mM dithiothreitol, 20 U ribonuclease inhibitor (Promega), and 200 U Superscript II RNase H^- Reverse Transcriptase (Invitrogen). The

resulting mix was incubated overnight at 37°C and then frozen at −80°C until PCR amplification.

Two steps of RT-mPCR (Ruano et al. 1995) were run to amplify 24 genes coding for the potassium channel subunits Kv1.2, Kv4.2, and Kv4.3; the calcium channel subunits α1A, α1B, α1C, α1D, α1E, α1G, α1H, and α1I; the hyperpolarization-activated channel subunits HCN1 and HCN2; the glutamate metabotropic receptor subunits mGluR3 and mGluR5; the neurotrypsin (Neuro.); the inhibitor of phosphatase 1 (I1); the protease Nexin 1 (PN1); the cholecystokinin (CCK); the polypeptidic complex IV of the cytochrome C oxidase (Cox-4); the homeodomain transcription factor Otx1; the transcriptional repressor Bcl 6; the calcium-binding protein calbindin 28K; and a substrate of the tyrosine kinase II (Ten-m3). The cDNAs present in the reverse transcription reaction were first amplified in a final volume of 100 μl with 0.2 μM of each of the 24 primer pairs (cf. Table 1), 2 mM of each of the deoxyribonucleotides triphosphates, 2.5 U *Taq* polymerase (Qiagen), and the buffer containing (in mM): 50 Tris (pH 8.9), 50 KCl, and 1.5 $MgCl_2$. Twenty PCR cycles (45 s at 94°C, 1 min 30 s at 56°C, 1 min at 72°C) were then performed, with an initial elongation period of 5 min at 94°C and a final one of 10 min at 72°C. Of this reaction, 2 μl was then used as a template for the second, gene-specific rounds of PCR. Each cDNA was individually amplified

TABLE 1. *List of the primers used to detect the mRNA expression of 24 genes in the two populations of layer V pyramidal cells by RT-PCR single cell*

Gene Name	Sense and Antisense Primer Sequences (Initial Position)	Primer Size, pb	Amplicon Size, pb	GenBank Reference
Kv1.2	GAG AAC CTC AGC TCC TGC CT (501)	20	590	M30440
	CTT CCT TGA TGT AGC CTT CAT (1523)	21		
Kv4.2	GTT ACC GTT TCG TGC GCA GT (751)	20	450	AF107780
	TAG CGC AAT GAC CAA GAC TC (1200)	20		
Kv4.3M/L	GAA GCT CCA ATG CCT ACC TG (1307)	20	421/478	AF107781
	CAA ATT AAG GCT GGA GCG AC (1728/1785)	20		
α1A	CAC TCA AGC TGG TGT CTG GA (467)	20	333	NM_007578
	GGA AAA CAG TGA GCA CAG CA (799)	20		
α1B	ACA TTC GTG GTC TCT CCA CC (4375)	20	306	NM_007579
	GAG GCG AAG GAAGCT TAG GT (4680)	20		
α1C	CCA GCC CAG AAA AGA AAC AG (3530)	20	271	NM_009781
	ACT GCC TTT TCC TTA AGG TGC A (3780)	22		
α1D	ATT GCC AGA AAA GAA AGC CTA GA (2450)	23	321	NM_028981
	AAT GAG CTT GTG GCA ACC CAC (2770)	21		
α1E	ATG GAG ACT CGG ACC AGA GC (509)	20	248	NM_009782
	GGT GGC CAG GAT CAT GTA CTC (757)	21		
α1G	GAT GGT ACC TCA CAC TGA GG (5916)	20	207	NM_009783
	GGT TGG GAG TGA ACA GAC AA (6122)	20		
α1H	AGG ACG CAG CAG AGT TTG AT (3753)	20	287	NM_021415
	GTT GGA GAC GCT GAG AAA GG (4029)	20		
α1I	ATG CTG GTG ATC CTG CTG AAC (79)	21	300	AF393329hu
	GCA CGC GGT TGA TGG CTT TGA G (400)	22		
HCN1	AGG TTA ATC AGA TAC ATA CAC C (1008)	22	231	AJ225123
	GAG TGC GTA GGA ATA TTG TTT T (1238)	22		
HCN2	CGG CTC ATC CGA TAT ATC CA (978)	20	230	AJ225122
	AGC GCG AAC GAG TAG AGC TC (1207)	20		
mGluR3	CAA GAA AAC ATC CCA CTG CTC A (767)	22	364	NM_181850
	TAG GAC TTG CGG ATG TTG GAG C (1131)	22		
mGluR5a/b	GCC TTC GTG CCT ATC TAC TTT G (2623)	22	377/473	NM_017012
	TTG GGG TTC TCC TTC TTG TTG A (2999)	22		Rat
Neurotrypsin	GAG AGG CCA CAG AAA ACA GC (1947)	20	337	Y13192
	AAG GTA CAA AAG CGG GGA CT (2283)	20		
I-1	CGA CAA CAG CCC ACG GAA GAT C (13)	22	486	AF281676
	GAA TCC AGT GGT AGC ATG TG (498)	20		
PN-1	CTT TCC TGT TTT CCA TCC GA (1272)	20	254	X70296
	GCC CTT TCT TCT GAC ACA GC (1525)	20		
CCK	CGC ACT GCT AGC GCG ATA CA (244)	20	217	NM_031161
	TTT CCT CAT TCC ACC TCC TC (460)	20		
COX4	ATG TTG GCT TCC AGA GCG CTG A (56)	22	507	M37829
	CTT CTT CCA CTC ATT CTT GTC ATA G (562)	25		
OTX1	GTT CGC AAA GAC TCG CTA CC (1659)	18	242	AF424700
	AAG CAG AGC TAG ATA CGGT CG (3211)	20		
Bcl6	TTC TTC CAG TTG CAG GCT TT (1210)	20	775	U41465
	TGC AGG AAG TTC ATC AAG GC (461)	20		
Calbindin-28K	GAC GGA AGT GGT TAC CTG GA (212)	20	416	NM_009788
	AGT TCC AGC TTT CCG TCA TTA (627)	21		
Ten-m3	ACC AAC GGG TGT CTG AAA AG (4868)	20	216	AB025412
	GTC CAC CGT GAT AGC CTT GT (5083)	20		

Detailed in this table are the abbreviated names of genes, the sequences of the sense and reverse primers given from the 5′ and 3′ and their initial position (number in parentheses), the size of the primer, the size of the PCR amplified product, and the accession number in GenBank. The amplified genes correspond to the potassium channel subunits Kv1.2, Kv4.2, and Kv4.3; the calcium channel subunits α1A, α1B, α1C, α1D, α1E, α1G, α1H, and α1I; the hyperpolarization-activated channel subunits HCN1 and HCN2; the glutamate metabotropic receptor subunits mGluR3 and mGluR5; the neurotrypsin (neuro.); the inhibitor of phosphatase 1 (1I); the protease nexin 1 (PN1); cholecystokinin (CCK); polypeptidic complex IV of the cytochrome C oxidase (Cox-4); orthodenticle homolog 1 (Otx-1); transcriptional repressor Bcl 6, calcium-binding protein calbindin 28K; and a substrate of the tyrosine kinase II (Ten-m3).

for 35 cycles using the same sets of primer pairs (cf. Table 1). The primers for α1C and α1D were not included in the initial experiments, which correspond to one third of the total number of tested cells.

Each PCR reaction (13 μl of the 100 μl reaction) was run on a 1.5% agarose gel stained with ethidium bromide, using a 100–base pair (bp) DNA ladder molecular weight marker (Promega). The efficiency of the RT-multiplex PCR protocol was tested on 500 pg total RNA from mouse cortex for each primer pair. The result of the PCR for each tested gene in all experiments was included in the database only when the positive control reaction (500 pg total rat brain RNA plus reverse transcriptase) demonstrated a single major band of correct size, whereas the negative control reaction (without reverse transcriptase) generated no detectable products other than primer dimers. The absence of contamination was verified with a negative control for which water was used as template, instead of single-cell cDNAs and with controls, with the contents of a pipette lowered in a slice with a positive pressure with which no cell was collected. All the PCR fragments amplified from mRNA spared at least one intron to prevent or at least identify amplification from genomic DNA. Additional measures were undertaken to diminish the possible occurrence of false negatives. First, to select the "healthiest" cells, PCR analyses were performed only on cells that had been recorded during the first 3 h that follow the preparation of the slices. We observed that the number of cells yielding positive PCR results and the number of amplified genes per cell tended to diminish after several hours in vitro (data not shown). The duration of the whole cell recordings before harvesting the cytoplasm was also kept as short as possible, usually <15 min. Finally, electrophysiological characteristics were used to select healthy cells to be included in the PCR database (stable resting membrane potential below −60 mV, input resistance >70 MΩ for mature animal and >200 MΩ for P5–7 mice, spontaneous synaptic potentials but no spontaneous action potentials, ability to emit repetitive action potentials on depolarizing current injection). Second, for all experiments positive controls (500 pg total rat brain RNA plus reverse transcriptase; see above) were tested for every primer pair in parallel with single-cell products. Third, only cells expressing at least two mRNA species were included. The average number of genes detected per cell was 5.8 ± 3.2.

RESULTS

Identification of CC-projecting and SC-projecting layer V neurons

To identify CC-projecting and SC-projecting neurons in layer V for subsequent experiments to compare their gene expression pattern and electrophysiological properties, the two populations were retrogradely labeled by injecting fluorescent beads in their specific axonal projection zones at P3–5 and observed 2–28 days later in acute slices of the visual and parietal associative cerebral cortices (Fig. 1, *inset*; see METHODS). At P21–30 fluorescent beads were localized exclusively in the soma of retrogradely labeled neurons. CC-projecting neurons had a widespread distribution consisting of layers II to VI (Fig. 1*B*), whereas SC-projecting neurons were localized in a restricted band in layer V (Fig. 1*C*). Retrograde labeling of the two populations in the same animal showed that within layer V, CC cells were predominantly superficial (layer Va; Fig. 1*D*) as previously reported (Ivy and Killackey 1982; Wise and Jones 1976), whereas SC cells were mainly localized deeper within the layer (layer Vb; Fig. 1*D*). This organization within layer V was less clear in P5–7 animals partly because fluorescent beads were not localized solely in the soma but were also found in the apical dendrites of retrogradely labeled cells (data not shown). All data described in the following sections were obtained from SC- or CC-projecting fluorescent pyramidal neurons located in layer V of the associative parietal and visual cortices.

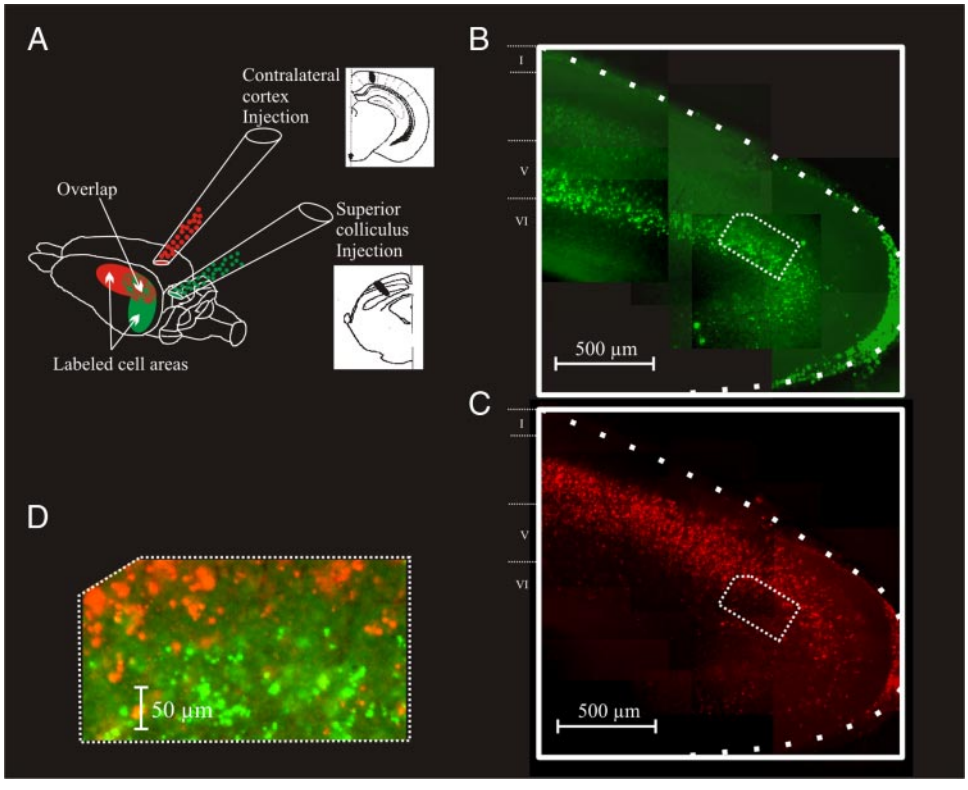

FIG. 1. Identification of 2 layer V pyramidal cell populations by retrograde labeling. *A*: scheme of the retrograde labeling procedure. Two black and white *insets* represent line drawings of injection sites in the contralateral cortex (*top inset*) and in the superior colliculus (*bottom inset*). *B* and *C*: photomontage (including the picture shown in *D*) illustrating the extent of the retrogradely labeled contralateral cortex (CC, red) and superior colliculus (SC, green) cells in the parietal associative and visual cortical areas. Note that SC cells were restricted to layer V, whereas CC cells were found in all layers except layer I. *D*: retrogradely transported fluorescent beads visualized in layer V of the visual cortex identifying pyramidal cells projecting to the contralateral cortex (CC cells, red beads) and to the superior colliculus (SC cells, green beads). Note the absence of double labeling and the preferential localization of SC cells in the lower part of layer V.

mRNA expression pattern of putative cell–specific markers in SC- and CC-projecting pyramidal neurons

We studied the expression pattern of 24 genes (see METHODS and Table 1 for the complete list) by single-cell RT-mPCR. These genes were primarily selected because they had been reported to be expressed in layer V but not in all neurons of this layer. They could thus potentially be selective markers of different populations of pyramidal cells. Although the main objective of the present analysis was not to correlate electrophysiological properties of pyramidal neurons with the expression pattern of specific genes, we also analyzed calcium channel subunit mRNAs because we hypothesized that bursting pyramidal neurons might express a specific set of calcium channels.

The products of the 24 selected genes could be amplified from total cortical RNA (Fig. 2*A*). The expression patterns of the 24 genes obtained by single-cell RT-mPCR in the two populations of pyramidal cells and at two developmental stages are shown in Fig. 2*B*. Most of the gene products had similar expression profiles in the four groups (i.e., young and mature CC- and SC-projecting neurons) with the following exceptions. The K^+ channel subunit Kv4.3 was the only gene that was preferentially expressed in CC-projecting neurons at the two developmental stages studied. The primers were designed to distinguish the short (Kv4.3M) and the long (Kv4.3L) splice variants (Liss et al. 2001; see Fig. 2*A* and Table 1). Kv4.3M was expressed in 23.1% of CC cells tested between postnatal days 5 and 7 (P5–7; $n = 12$) and 30.4% of the CC cells tested at P21–30 ($n = 24$), whereas Kv4.3M transcripts were not observed in SC cells at P5–7 ($n = 11$) and in only 6.25% of the SC cells at P21–30 (one out of 16 tested neurons). Kv4.3L was never detected excepted in one mature CC cells for which it was coexpressed with Kv4.3M. These observations suggest that CC and SC cells already differ in their gene expression pattern as early as during the first postnatal week. The expression of four other genes was differentially regulated in CC and SC cells during postnatal development. Two genes encoding the calcium channel subunits α1B and α1C were expressed at P5–7 in CC cells (α1B: 18.5%; $n = 16$ and α1C: 41.7%; $n = 12$) and in SC cells (α1B: 27.3%, $n = 11$; and α1C: 50%, $n = 11$) as well as at P21–30 in CC cells (α1B: 12.5%, $n = 24$; and α1C: 54.5%, $n = 11$). In contrast, neither α1B ($n = 16$) nor α1C ($n = 12$) was expressed in SC cells at P21–30. Calbindin mRNAs were rarely detected in cells from P5–7 mice (CC cells: 0%, $n = 16$; and SC cells: 9%, $n = 11$), whereas they were expressed in 33.3% of CC cells ($n = 24$) but in none of the SC cells ($n = 16$) of more mature animals. Finally, protease nexin 1 (PN1) transcripts were detected in 37.5% of CC cells ($n = 16$) at P5–7 but in none of the CC cells at P21–30 ($n = 24$). This gene was detected in SC cells at both developmental stages (P5–7: 36.4%, $n = 11$; P21–30: 25%, $n = 16$). The other genes had either a similar level of expression in the two populations at both developmental stages or were expressed in <20% of the cells in each group and will not be discussed further.

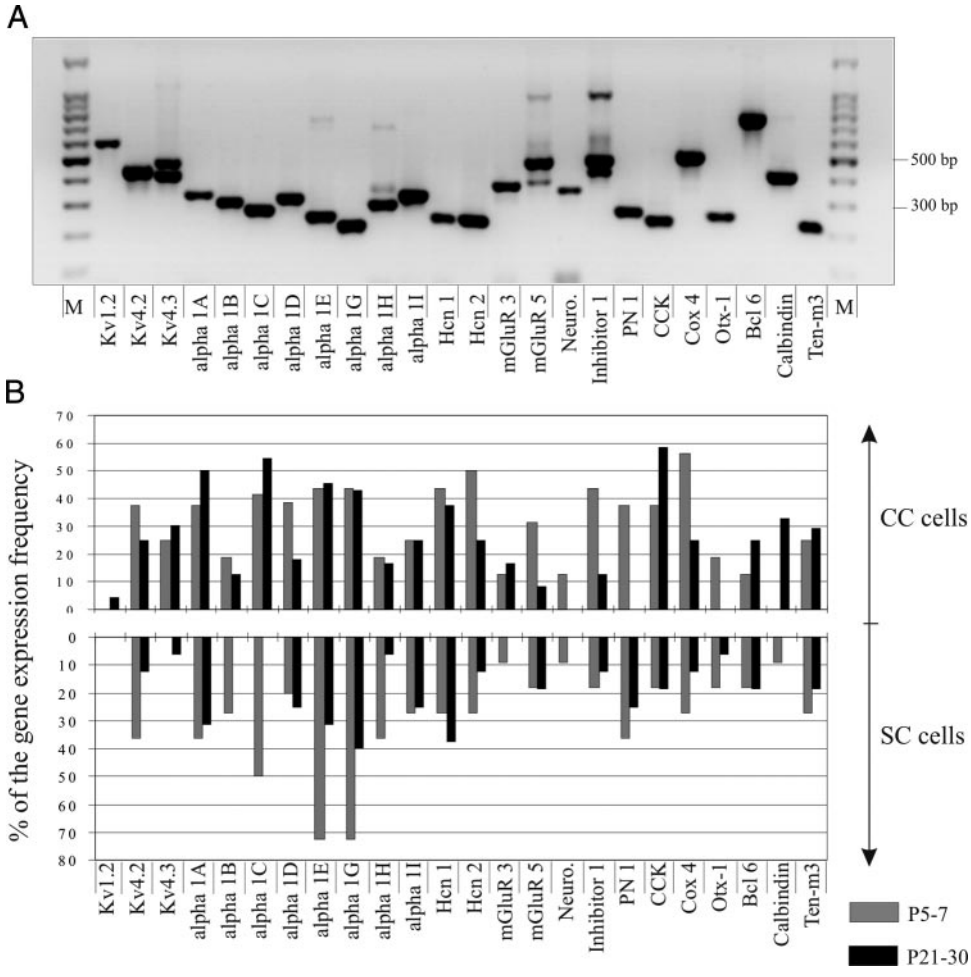

FIG. 2. Single-cell RT-PCR analysis of the expression pattern of 24 genes in CC and SC cells during the first (P5–7) and fourth (P21–30) postnatal week. *A*: agarose gel electrophoresis of the products obtained from 500 pg of total brain RNA with the RT-PCR procedure design to coamplify simultaneously the 24 mRNAs. For each gene, an amplification product of the expected size (see Table 1) was obtained ("M": 100-bp DNA ladder molecular weight markers, with position of 500- and 300-bp bands indicated on the *right*. *B*: percentages of CC (*top*) and SC (*bottom*) cells expressing each of 24 genes analyzed at P5–7 (gray bars) and P21–30 (black bars). Number of cells included in the analysis was: 16 for P5–7 CC cells except for Kv4.3 ($n = 12$), alpha1C and -D ($n = 12$); 11 for P5–7 SC cells except for alpha1C and -D ($n = 10$); 24 for P21–30 CC cells except for Kv4.3 ($n = 23$), alpha1C and -D ($n = 11$), alpha1E ($n = 22$), alpha1G ($n = 21$); 16 for P21–30 SC cells except for alpha1C and -D ($n = 12$), alpha1G ($n = 15$).

TABLE 2. *Passive and active electrophysiological characteristics of the two populations of layer V pyramidal cells (CC- and SC-projecting neurons) at two developmental stages (P5–7 and P21–30)*

	P5–7 CC cells	P5–7 SC cells	P21–30 CC cells	P21–30 SC cells
Resting potential, mV	−68.3 ± 1.3 (n = 19)	−68.5 ± 1.7 (n = 18)	−76.6 ± 1.5 (n = 25)	−75.3 ± 1.5 (n = 18)
Input resistance, MΩ	424.5 ± 41.6 (n = 19)	309.3 ± 21.7* (n = 18)	156.8 ± 7.7 (n = 25)	115.5 ± 9.2* (n = 18)
Amplitude of 1h rectification, mV	4.6 ± 0.6 (n = 19)	10.0 ± 1.0** (n = 18)	2.5 ± 0.3 (n = 25)	5.1 ± 0.4** (n = 18)
Action potential threshold, mV	−40.0 ± 1.0 (n = 19)	−42.6 ± 0.6* (n = 18)	−45.9 ± 0.8 (n = 25)	−52.5 ± 0.6** (n = 18)
Action potential amplitude, mV	67.6 ± 1.4 (n = 19)	70.7 ± 1.8 (n = 18)	83.7 ± 1.4 (n = 25)	88.9 ± 1.2* (n = 18)
Duration at midheight, ms	1.8 ± 0.1 (n = 19)	2.0 ± 0.1 (n = 18)	0.80 ± 0.03 (n = 25)	0.80 ± 0.03 (n = 18)
Duration at threshold, ms	3.9 ± 0.2 (n = 19)	4.3 ± 0.3 (n = 18)	1.80 ± 0.09 (n = 25)	1.80 ± 0.08 (n = 18)
Frequency adaptation, %	40.2 ± 3.9 (n = 8)	32.8 ± 4.1 (n = 8)	77.3 ± 2.2 (n = 7)	76.7 ± 1.6 (n = 8)

Statistics correspond to the comparison of the two populations at a given developmental stage. *$P < 0.05$; ** $P < 0.001$. See RESULTS for more statistics and METHODS for determination of the parameters.

Developmental changes of intrinsic membrane properties of CC- and SC-projecting pyramidal cells

We also studied intrinsic membrane properties (see METHODS) of SC and CC cells at P5–7 and P21–30 and we observed developmental changes of several characteristics in the two populations. The following comparisons are based on the analysis of 19 P5–7 and 25 P21–30 CC and 18 P5–7 and 18 P21–30 SC cells unless otherwise stated (see also Table 2 and Figs. 3, 4, and 5).

Subthreshold membrane properties

The resting membrane potentials of CC and SC cells were comparable at both developmental stages and shifted from −68.4 ± 1.5 mV at P5–7 to −76.0 ± 1.5 mV at P21–30 (P = 0.0003). The input resistance (Ri) of pyramidal cells decreased between the first and the third postnatal weeks (Fig. 3, *A*, *B*, and *C*; $P < 0.0001$). For CC cells, Ri decreased from 424.5 ± 41.6 MΩ at P5–7 to 156.8 ± 7.7 MΩ at P21–30 and for SC cells it decreased from 309.3 ± 21.7 MΩ at P5–7 to 115.5 ± 9.19 MΩ at P21–30. SC neurons had a significantly lower Ri than that of CC cells at P5–7 (Fig. 3, *A1*, *A2*, and *C*; $P < 0.025$) and at P21–30 (Fig. 3, *B1*, *B2*, and *C*; $P < 0.005$).

Neurons from both populations exhibited a hyperpolarization-activated current (Ih) responsible for the sag of potential observed in response to hyperpolarizing current pulses (Figs. 3 and 4). The amplitude of the sag measured between the peak of hyperpolarizations reaching an initial potential of 105 ± 5 mV

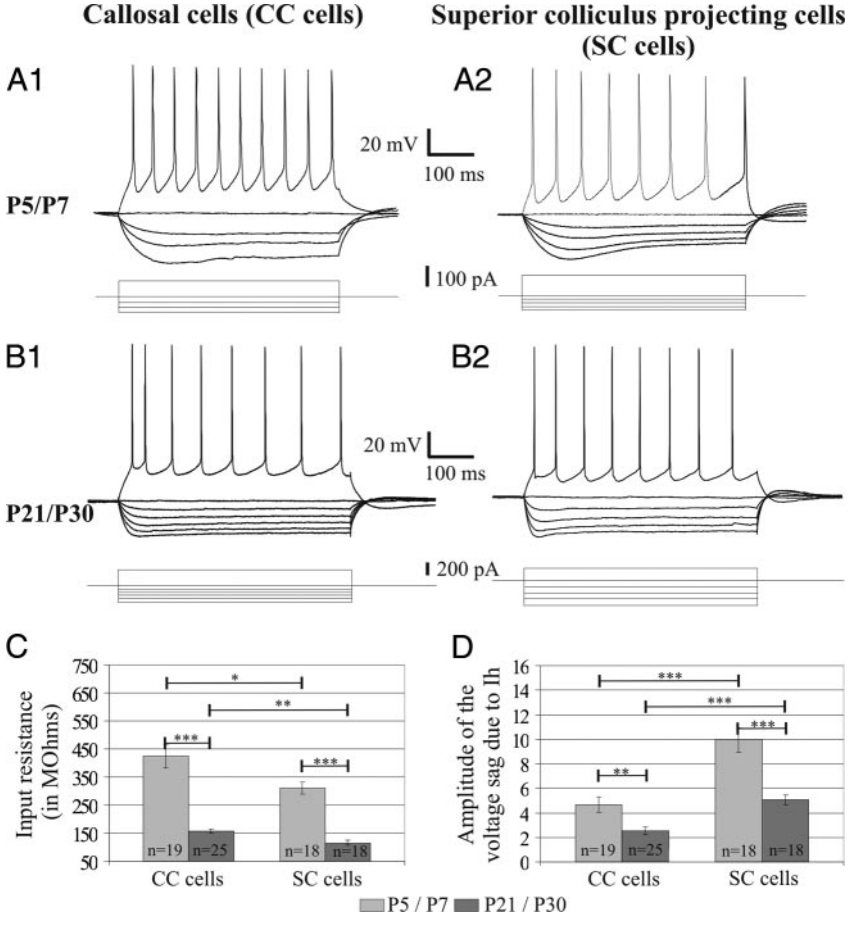

FIG. 3. Developmental changes in the intrinsic membrane properties of layer V neurons projecting to the contralateral hemisphere through corpus callosum (CC neurons) or to the superior colliculus (SC neurons). *A* and *B*: action potential discharges and subthreshold membrane properties of a P5 CC neurons (*A1*), a P5 SC neuron (*A2*), a P25 CC neuron (*B1*), and a P27 SC neuron (*B2*). *C*: comparison of the input resistance of CC cells (*left histogram*) and SC cells (*right histogram*) at P5–7 (gray bars) and at P21–30 (black bars) (*P = 0.02; **$P < 0.002$; ***$P < 0.0001$). *D*: comparison of the amplitude of the voltage sag resulting from the activation of the hyperpolarization-activated current (Ih) measured between the initial peak of hyperpolarizing responses to −105 ± 5 mV and the plateau at the end of the response for CC and SC cells at the 2 developmental stages (**$P < 0.005$; ***$P <$ 0.0005).

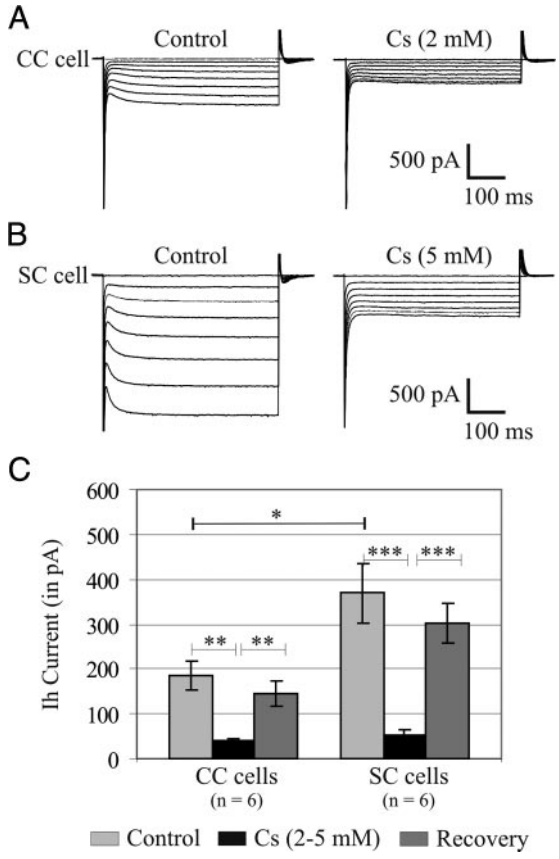

FIG. 4. Comparison of the Ih currents in CC and SC cells. *A* and *B*: voltage-clamp recordings showing the current responses to hyperpolarizing voltage steps from −60 to −130 mV of one CC neuron (*A*) and one SC neuron (*B*) at P21 in control conditions (*left*) and in the presence of cesium in the extracellular solution (*right*). *C*: comparison between mature (P21–30) CC and SC cells of the amplitude of Ih currents induced by hyperpolarizations to −130 mV and measured between the initial value of the current extrapolated at the beginning of the step (see METHODS) and the plateau just before the end of the pulse, in control conditions, after the addition of cesium and after recovery (*$P = 0.03$; **$P < 0.005$; ***$P < 0.001$).

and the plateau at the end of the responses decreased with age in CC cells (Fig. 3, *A1*, *B1*, and *D*; $P < 0.005$) as in SC cells (Fig. 3, *A2*, *B2*, and *D*; $P = 0.0005$). Furthermore, the amplitude of the sag was greater in SC cells than in CC cells both at P5–7 (Fig. 3, *A1*, *A2*, and *D*; $P < 0.0001$) and at P21–30 (Fig. 3, *B1*, *B2*, and *D*; $P = 0.0001$).

Additional experiments were performed in voltage-clamp mode and in the presence of tetrodotoxin (TTX) to compare more directly Ih in the two populations of pyramidal cells. Activation of Ih was induced by applying hyperpolarizing voltage commands of increasing amplitude from a holding potential of −60 mV. Inward currents that slowly developed during the hyperpolarizing commands were reversibly blocked by cesium (Cs, 2–5 mM) in CC ($n = 6$) and SC ($n = 6$) cells (Fig. 4, *A* and *B*), confirming the involvement of Ih. In the presence of Cs, the current–voltage relationship obtained at hyperpolarized potentials presented an inward rectification (not shown but see the *right panels* of Fig. 4, *A* and *B*) probably arising from the voltage-dependent block of potassium currents by external Cs (Brunton and Charpak 1998; Hagiwara et al. 1976). Activation curves of the Ih currents did not differ between CC and SC cells (data not shown), although the amplitude of Ih at −130 mV in mature SC cells (368.6 ± 65.7 pA, $n = 6$) was on average twice that of CC cells (184.7 ± 31.7 pA, $n = 6$; Fig. 4*C*; $P = 0.03$).

Action potential characteristics

The threshold, amplitude, and duration of the first action potential of a discharge at 10.8 ± 1.1 Hz induced by a depolarizing step of current (Fig. 3, *A* and *B*) were measured in CC and SC cells at the two ages. The action potential threshold shifted from −40.0 ± 1.0 to −45.9 ± 0.8 mV in CC cells (Fig. 3, *A1* and *B1* and Fig. 5*A*; $P < 0.0001$) and from −42.6 ± 0.6 to −52.5 ± 0.6 mV in SC cells (Fig. 3, *A2* and *B2* and Fig. 5*A*; $P < 0.0001$) between the first and the third postnatal weeks. SC cells thus had a slightly more hyperpolarized action potential threshold than CC cells at P5–7 (Fig. 3, *A1* and *A2* and Fig. 5*A*; $P = 0.0384$) and this difference became most significant in mature mice (Fig. 3, *B1* and *B2* and Fig. 5*A*; $P < 0.0001$). Between these two ages, the action potential amplitude increased from 67.6 ± 1.4 to 83.7 ± 1.4 mV in CC cells (Fig. 3, *A1* and *B1* and Fig. 5*B*; $P < 0.0001$) and from 70.7 ± 1.8 to 88.9 ± 1.2 mV in the SC cells (Fig. 3, *A2* and *B2* and Fig. 5*B*; $P < 0.0001$). This parameter was significantly different be-

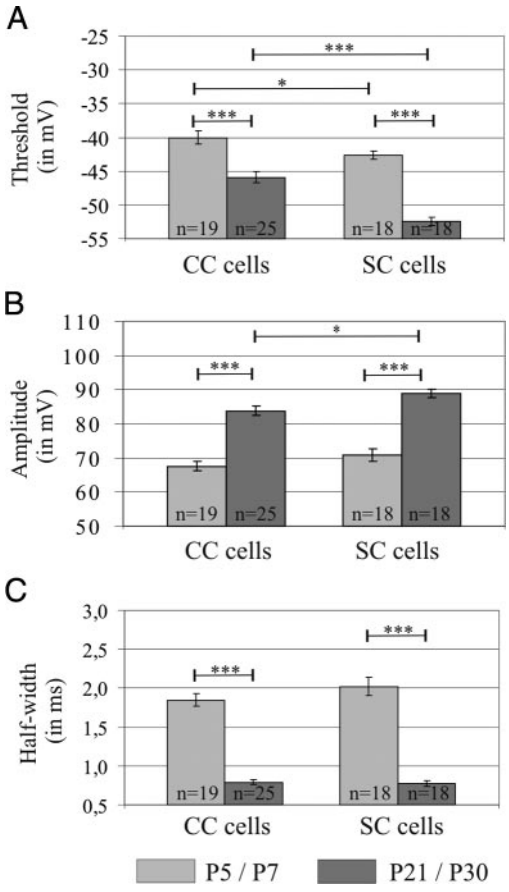

FIG. 5. Developmental changes of action potential (AP) characteristics of CC and SC cells. *A*: action potential threshold (*$P < 0.05$; ***$P < 0.0001$). *B*: action potential amplitude (*$P < 0.02$; ***$P < 0.0001$). *C*: action potential duration at half height (***$P < 0.0001$). All values were obtained from the first action potential of discharge with a mean frequency of 10.8 ± 1.1 Hz induced by depolarizing current pulses from rest. Note that CC neurons have a higher threshold than SC neurons at the 2 developmental stages and that AP amplitude of CC neurons was lower than that of SC neurons in mature animals.

tween CC and SC cells only in mature animals (Fig. 3, *A2* and *B2* and Fig. 5*B*; $P = 0.015$). Moreover, action potential duration measured at midheight decreased from 1.80 ± 0.10 to 0.80 ± 0.03 ms in CC cells (Table 2; Fig. 5*C*; $P < 0.0001$) and from 2.00 ± 0.10 to 0.80 ± 0.03 ms in SC cells (Table 2; Fig. 5*C*; $P < 0.0001$), although the values of this parameter at a given developmental stage did not differ between both populations.

Effects of in vivo anesthesia on the proportions of bursting cells recorded in vitro

In our initial experimental conditions, the period between the induction of the anesthesia with the intraperitoneal injection of a mixture of ketamine and xylazine (see METHODS) and the decapitation usually did not exceed 2 min. Under these conditions, CC and SC pyramidal cells of mature animals did not display differences in their action potential firing behavior. Neurons from both populations showed regular firing discharges (Fig. 6, *A1* and *B1*) and no significant differences were observed in their discharge frequencies. The frequency adaptation observed during discharges elicited by depolarizing pulses of 500-ms duration (see METHODS) was 77.3 ± 2.2% for CC-projecting neurons ($n = 7$) and 76.7 ± 1.6% for SC-projecting neurons ($n = 8$; $P = 0.8$). It is worth noting that frequency adaptation was also identical between the two groups of projecting neurons at P7 (40.2 ± 3.9% for CC cells, $n = 8$, and 32.8 ± 4.1% for SC cells, $n = 8$; $P = 0.2$). The regular firing behavior of mature SC pyramidal cells was a surprising observation because it has been previously reported that these neurons switched from a regular to a bursting mode of firing during the third postnatal week, whereas CC cells maintained a regular firing mode throughout the first five postnatal weeks (Kasper et al. 1994c).

The ability of large layer V pyramidal neurons to fire complex bursts of action potential relies partly on the presence of a calcium spike initiation zone in their apical dendrite (Larkum et al. 1999b; Stuart and Hausser 2001). The absence of bursting behavior in SC cells could have been caused by the damage of their prominent apical dendrites during the slicing procedure. This was unlikely, however, because 11 of 15 SC cells that fired regularly and were labeled with the fluorescent dye Alexa Fluor 568 clearly displayed apical dendrites in layer I where they formed a typical tuft (data not shown).

When the duration of the period between the induction of the anesthesia with the intraperitoneal injection of a mixture of ketamine and xylazine and the decapitation was increased up to 4–10 min, we observed that some SC cells displayed a bursting behavior in P21–30 animals. Indeed, one third of 27 SC cells tested after prolonged anesthesia with ketamine and xylazine fired an initial burst of action potentials in response to a depolarizing pulse of current (Fig. 6, *C2* and *C3*). The other SC cells fired regularly as did all but one of the tested CC cells ($n = 22$). To investigate whether another type of anesthetics could influence the firing behavior of pyramidal neurons, we used pentobarbital to anesthetize mature mice for more than 4 min before decapitation. Of all the SC cells tested ($n = 14$), six fired with an initial burst (43%; Fig. 6*C3*), whereas eight cells had regular discharges of action potentials (57%; Fig. 6*B3*). All nine tested CC cells fired regularly (Fig. 6*A3*). Prolonged anesthesia with ketamine and xylazine or pentobarbital did not significantly affect the resting membrane potential or the input resistance of CC cells. However, bursting SC cells (recorded after a prolonged anesthesia with either of the two anesthetics) had a lower input resistance (85.2 ± 6.5 MΩ; $n = 15$) than the nonbursting SC cells recorded under the same conditions (107.4 ± 8.7 MΩ, $n = 22$; $P < 0.05$) or the SC cells recorded after a short anesthesia with ketamine and xylazine (115.5 ± 9.4, $n = 18$, $P < 0.02$). Bursting SC cells also had action potentials of shorter duration (0.63 ± 0.02 ms, $n = 15$) than nonbursting SC cells recorded under the same conditions

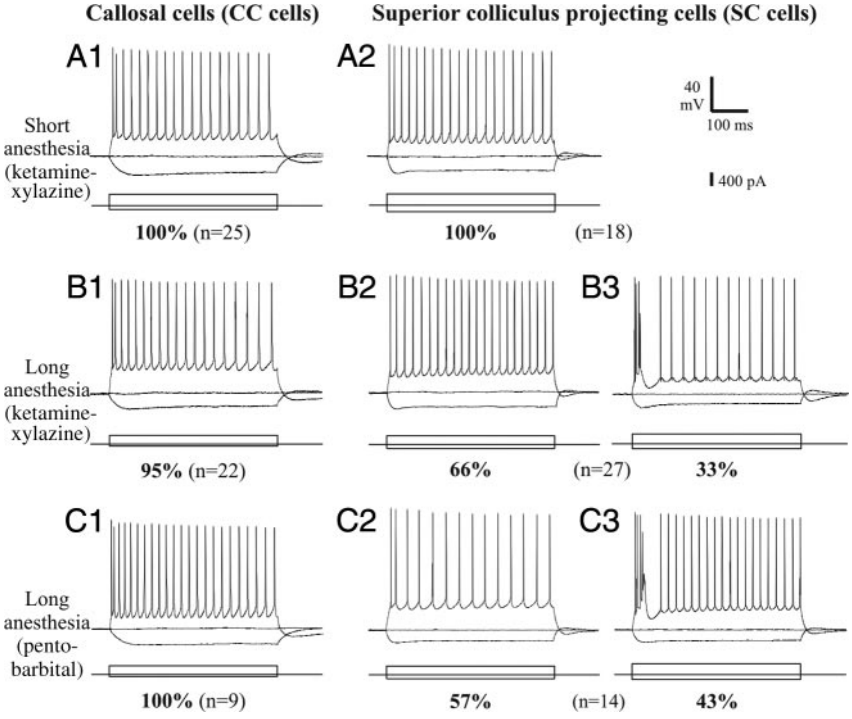

FIG. 6. Duration of anesthesia influences the action potential firing behavior of SC-projecting neurons recorded in vitro. *A* and *B:* P21 mice were anesthetized with ketamine–xylazine either for a short (<2 min) or a long (4–10 min) period of time before decapitation. Similar regular firing discharges were observed in CC cells in both conditions (*A1* and *B1*). All SC cells recorded from slices obtained after a short duration of anesthesia also fired regularly (*A2*), whereas after a prolonged anesthesia 33% of the SC cells were able to fire bursts of action potentials at the onset of a depolarizing pulse (*B3*). *C*: bursting behavior was also observed for SC cells (*C2* and *C3*) but not in CC cells (*C1*) after a prolonged anesthesia with the other anesthetic pentobarbital at P21–30.

(0.77 ± 0.05 ms, $n = 22$; $P = 0.011$) as well as SC cells recorded after a short anesthesia with ketamine and xylazine (0.77 ± 0.04, $n = 18$, $P = 0.002$).

The induction of a bursting behavior in a significant proportion of SC cells recorded in vitro after a prolonged anesthesia could result from a direct and irreversible effect of the anesthetics on the intrinsic membrane properties of the recorded cells. We therefore tested whether the firing discharges of SC cells recorded in vitro after a short anesthesia were modulated by bath application of anesthetics in the extracellular recording solutions. Only two of 21 SC cells showed a transition from regular to bursting firing after bath application of ketamine (10–200 μM) and none with bath application of a mixture of ketamine and xylazine (200 μM/50 μM; $n = 3$) or of pentobarbital (15–100 μM; $n = 5$; data not shown). This suggests that the effects of prolonged anesthesia on the firing behavior of SC cells did not result simply from a direct block or enhancement of a conductance expressed in SC cells by anesthetics.

DISCUSSION

The single-cell RT-PCR analysis performed in the present study aimed primarily at identifying genes that might be selectively expressed in either CC- or SC-projecting neurons of layer V. However, our results indicate that CC and SC cells had similar mRNA expression patterns for most of the 24 genes studied. Before discussing the observations highlighting the few genes that we found to be differentially expressed in the two populations at different stages of the postnatal development, it must be kept in mind that our PCR analysis gives only qualitative information on the expression pattern of mRNAs present mostly in the soma of the recorded neurons. A quantitative analysis that would be required to correlate unambiguously quantitative differences in the functional properties of CC- and SC-projecting neurons with the expression level of specific genes was beyond the scope of the present study (for a recent review see Liss and Roeper 2004). Kv4.3 mRNA has a relatively weak expression in the entire neocortex (Serodio and Rudy 1998) but we found that it was expressed in a subset of CC cells, suggesting that Kv4.3 probably contributes to A-type potassium currents previously described in CC cells (Locke and Nerbonne 1997). This preferential expression of Kv4.3 in a subset of CC cells does not exclude the presence of A-type potassium currents in other CC cells or in SC cells because other different subunits can be combined to form the channels responsible for this type of currents (reviewed in Song 2002). Interestingly, the preferential expression of Kv4.3 in CC-projecting neurons was observed as early as at P5–7, which indicates that the expression of the molecular determinants of some of the CC and SC cell functional characteristics already mature differentially before the end of the first postnatal week. Apart from Kv4.3, none of the tested genes could be used as a specific and selective marker for any of these two populations throughout development.

Nevertheless, we observed some differences between CC and SC cells in the postnatal development of their expression pattern of the calcium channel subunits α1B (Cav2.2) and α1C (Cav1.2). Our single-cell RT-PCR data showed that the expression of these two subunits is selectively down-regulated in SC cells of mature animals, which suggests a lower contribution of N- and L-type calcium channels in mature SC cells as compared with mature CC cells and immature SC and CC pyramidal neurons. Interestingly, Stewart and Foehring (2000) observed that the N- and L-type channels had a lower percentage contribution to the total calcium currents recorded in SC cells than in CC cells dissociated from mature rats (3 to 7 wk old). This differential expression of α1B (Cav2.2) and α1C (Cav1.2) in mature CC- and SC-projecting neurons is not accompanied by a clear difference in the action potential firing behavior of these two cell types, suggesting that other calcium channel subunits also contribute to the calcium-dependent regulation of the repetitive firing of pyramidal cells. Finally, during the first postnatal week both CC and SC cells expressed mRNAs coding for protease nexin 1 (PN1) whereas, after the third postnatal week, PN1 expression was restricted to a subpopulation of SC cells. PN1 is a serine protease inhibitor expressed in various brain areas and in particular layer V neurons of the neocortex (Simpson et al. 1994). It has been proposed that PN1 could prevent the inhibition of neurite outgrowth caused by thrombin and other serine proteases (Turgeon et al. 1998). It is thus tempting to hypothesize that the differential expression of PN1 by CC and SC cells is related to the differential maturation of their apical tuft (retraction vs. maintenance). However, this seems unlikely because preliminary data indicate that CC cells still express PN1 between P15 and P20, i.e., more than a week after the completion of their apical tuft retraction. Therefore the expression pattern of PN1 during postnatal development is most probably related to other aspects of the dendritic maturation of pyramidal cells than the apical tuft retraction. Calbindin mRNAs were rarely detected in any cells from P5–7 mice, whereas in more mature animals they were expressed in 30% of CC cells but in none of the SC cells. In conclusion, the comparison between CC and SC cells of the expression pattern of a restricted number of genes did not allow the identification of molecular markers specific for an entire cell population throughout development. However, expression of specific mRNAs is differentially regulated between the two populations as early as during the first postnatal weeks (Kv4.3) or later on during the postnatal development (α1B, α1C, PN1, and calbindin).

Our results on the postnatal development of electrophysiological properties of mouse CC and SC cells are in accordance with previous studies performed on layer V pyramidal cells of visual, sensorimotor, and prefrontal areas of the rat neocortex (Franceschetti et al. 1998; Kasper et al. 1994b; McCormick and Prince 1987; Zhang 2004; Zhu 2000). In all cases, maturation of pyramidal cells during the first four postnatal weeks is accompanied by a continuous shift of the resting membrane potential and of the action potential threshold toward more hyperpolarized values, a decrease of input resistance and of action potential duration, and an increase in action potential amplitude. As already discussed (Zhang 2004), quantitative differences among these various studies for some parameters, and in particular for the input resistance and the resting membrane potential at early postnatal stages, are probably a consequence of the different recording techniques used and of the lower leak current obtained with patch-clamp recordings as opposed to recordings with sharp electrodes (Spruston and Johnston 1992). Accordingly, our measurements of these electrophysiological parameters compare favorably with those of

Zhang (2004) performed by means of whole cell recordings in the rat neocortex.

We did not observe any major qualitative difference between intrinsic membrane properties of CC- and SC-projecting neurons during the postnatal development. However, our results confirmed the existence of quantitative differences between the electrophysiological characteristics of these two cell types in mature animals. Indeed, we observed that, in mice, mature SC cells have a lower input resistance, a more pronounced Ih current, a lower action potential threshold, and action potentials of larger amplitude than those of mature CC neurons. These results are in line with previous studies that directly compared SC and CC cells in rats (Kasper et al. 1994a; Solomon et al. 1993) and those that compared layer V pyramidal cells with (putative subcortical projecting cells) or without (putative CC cells) an apical tuft in layer I (Hefti and Smith 2000; Mason and Larkman 1990; Yang et al. 1996). Our study further reveals that most of these functional differences are already expressed before the end of the first week of postnatal development. Whole cell recordings from slices of P5 to P7 animals showed that SC cells have a lower input resistance, a more pronounced Ih, and a lower threshold for action potentials than CC cells. These differences had not been reported by Kasper et al. (1994b,c). It is possible that such differences are species specific, or the result of different methods of recording (patch-clamp and sharp electrodes), or explained by the fact that Kasper et al. (1994b,c) could not record from retrogradely labeled neurons as early as at P5–7. Nevertheless, our results indicate that functional differences between CC and SC cells are specified much earlier than previously thought (Kasper et al. 1994b,c). Rather than a sequential maturation consisting of an early morphological dendritic maturation followed by a later differentiation of electrophysiological characteristics, our results favor the hypothesis that both morphological and electrical properties of layer V evolve simultaneously, as early as from the first postnatal week, to achieve the different phenotypes observed in mature CC and SC cells.

Surprisingly, the most striking functional difference between CC and SC cells that had been reported previously, i.e., the acquisition of a bursting behavior by SC cells during the third postnatal week (Kasper et al. 1994c), could be affected by anesthesia. After the injection of the anesthetics, usually about 1 min is required to abolish all noxious reflexes. When the period of anesthesia performed before sacrificing the animals was within 2 min, all CC and SC cells fired action potentials regularly at all stages. The bursting behavior was observed in one third of the SC cells when the duration of the anesthesia was increased. In both conditions, more than 95% of CC cells continued to fire regularly. Despite considerable efforts, we could not induce a bursting behavior of SC cells systematically by applying the anesthetics in vitro and this prevented us from analyzing the mechanisms of action (for review, see Antkowiak 2001). However, the induction of a bursting behavior was also accompanied by a reduction of the input resistance and of the action potential duration in bursting SC cells compared with regular spiking SC cells (recorded either after a short or a prolonged anesthesia).

These observations do not support the hypothesis of a down-regulation of Ih to explain the effects of anesthetics. Indeed, Ih channels which have a higher density in the distal apical dendrites than in the proximal dendrites or in the soma of large layer V pyramidal cells (Berger et al. 2001; Lorincz et al. 2002; Williams and Stuart 2000) can influence their firing behavior toward a regular or a bursting mode by modulating the coupling between somatic and dendritic spike initiation zones (Berger et al. 2003). The pharmacological blockade of Ih channels in pyramidal cells favors the induction of dendritic calcium spikes and therefore of a bursting behavior in response to somatic depolarization (Berger et al. 2003). However, this inhibition of Ih is usually accompanied by an increase in the apparent input resistance measured in the soma of hippocampal and neocortical pyramidal neurons (Berger et al. 2001, 2003; Magee et al. 1998).

Therefore our results suggest that the effects of anesthetics involve the opening of a conductance that depolarizes the dendrite and thereby facilitates the triggering of dendritic calcium spikes on back-propagation of somatic action potentials (Berger et al. 2003; Franceschetti et al. 1995; Larkum et al. 1999a; Schwindt and Crill 1999). The higher proportion of bursting SC cells in slices obtained from deeply anesthetized animals is reminiscent of in vivo studies in the neocortex reporting higher percentages of bursting neurons in anesthetized than in nonanesthetized animals (Steriade et al. 2001, 2004). As proposed by Steriade (2004), these observations might indicate that the intrinsic membrane properties are overwhelmed by the high levels of synaptic activity in the intact brain (also see Degenetais et al. 2002; Mahon et al. 2001; Paré et al. 1998). The transition from one firing mode to another (including regular spiking to burst firing) for a given cell can occur during transitions between different brain states (Steriade et al. 2001), suggesting that variations in synaptic activity and membrane potential observed in different brain states, including anesthetized states, impose the mode of discharge of neurons. Obviously, the situation is different in vitro because both regular spiking and bursting layer V SC cells can be recorded in the presence of glutamate and γ-aminobutyric acid type A ($GABA_A$) receptors antagonists, which substantially reduced the impact of synaptic activity (data not shown). Our results therefore indicate that long anesthesia induces a long-term modification of some ion channels underlying intrinsic membrane properties of SC cells. However, this does not exclude the involvement of network activities in the induction of this modification, which would explain why it is not easily reproducible in vitro.

ACKNOWLEDGMENTS

We thank F. Nadrigny and M. Oheim for help with imaging and for material loaning, A. Roebuck for performing preliminary RT-PCR experiments, and M. Hanafi for technical assistance. We are grateful to A. Chung and R. Rolph for comments on the manuscript.

Present addresses: E. Audinat and S. Charpak, INSERM U603, CNRS FRE2500, Université Paris 5, 45 rue des StPères, 75006 Paris, France; N. Doerflinger, INSERM U371, 18, avenue du Doyen Lépine, 69500 Bron, France.

GRANTS

This work was supported by the Human Frontier Science Program (RG 107/2001), the Avenir program of the Institut National de la Santé et de la Recherche Médicale, and the Fondation pour la Recherche Médicale (INE20001117003/1 and FDT20030627228).

REFERENCES

Antkowiak B. How do general anaesthetics work? *Naturwissenschaften* 88: 201–213, 2001.

Berger T, Larkum ME, and Luscher HR. High I(h) channel density in the distal apical dendrite of layer V pyramidal cells increases bidirectional attenuation of EPSPs. *J Neurophysiol* 85: 855–868, 2001.

Berger T, Senn W, and Luscher HR. Hyperpolarization-activated current Ih disconnects somatic and dendritic spike initiation zones in layer V pyramidal neurons. *J Neurophysiol* 90: 2428–2437, 2003.

Brunton J and Charpak S. mu-Opioid peptides inhibit thalamic neurons. *J Neurosci* 18: 1671–1678, 1998.

Cauli B, Audinat E, Lambolez B, Angulo MC, Ropert N, Tsuzuki K, Hestrin S, and Rossier J. Molecular and physiological diversity of cortical nonpyramidal cells. *J Neurosci* 17: 3894–3906, 1997.

Cauli B, Porter JT, Tsuzuki K, Lambolez B, Rossier J, Quenet B, and Audinat E. Classification of fusiform neocortical interneurons based on unsupervised clustering. *Proc Natl Acad Sci USA* 97: 6144–6149, 2000.

Degenetais E, Thierry AM, Glowinski J, and Gioanni Y. Electrophysiological properties of pyramidal neurons in the rat prefrontal cortex: an in vivo intracellular recording study. *Cereb Cortex* 12: 1–16, 2002.

Franceschetti S, Buzio S, Sancini G, Panzica F, and Avanzini G. Expression of intrinsic bursting properties in neurons of maturing sensorimotor cortex. *Neurosci Lett* 162: 25–28, 1993.

Franceschetti S, Guatteo E, Panzica F, Sancini G, Wanke E, and Avanzini G. Ionic mechanisms underlying burst firing in pyramidal neurons: intracellular study in rat sensorimotor cortex. *Brain Res* 696: 127–139, 1995.

Franceschetti S, Sancini G, Panzica F, Radici C, and Avanzini G. Postnatal differentiation of firing properties and morphological characteristics in layer V pyramidal neurons of the sensorimotor cortex. *Neuroscience* 83: 1013–1024, 1998.

Hagiwara S, Miyazaki S, and Rosenthal NP. Potassium current and the effect of cesium on this current during anomalous rectification of the egg cell membrane of a starfish. *J Gen Physiol* 67: 621–638, 1976.

Hallman LE, Schofield BR, and Lin CS. Dendritic morphology and axon collaterals of corticotectal, corticopontine, and callosal neurons in layer V of primary visual cortex of the hooded rat. *J Comp Neurol* 272: 149–160, 1988.

Hefti BJ and Smith PH. Anatomy, physiology, and synaptic responses of rat layer V auditory cortical cells and effects of intracellular GABA(A) blockade. *J Neurophysiol* 83: 2626–2638, 2000.

Hevner RF, Daza RA, Rubenstein JL, Stunnenberg H, Olavarria JF, and Englund C. Beyond laminar fate: toward a molecular classification of cortical projection/pyramidal neurons. *Dev Neurosci* 25: 139–151, 2003.

Ivy GO and Killackey HP. Ontogenetic changes in the projections of neocortical neurons. *J Neurosci* 2: 735–743, 1982.

Kasper EM, Larkman AU, Lubke J, and Blakemore C. Pyramidal neurons in layer 5 of the rat visual cortex. I. Correlation among cell morphology, intrinsic electrophysiological properties, and axon targets. *J Comp Neurol* 339: 459–474, 1994a.

Kasper EM, Larkman AU, Lubke J, and Blakemore C. Pyramidal neurons in layer 5 of the rat visual cortex. II. Development of electrophysiological properties. *J Comp Neurol* 339: 475–494, 1994b.

Kasper EM, Lubke J, Larkman AU, and Blakemore C. Pyramidal neurons in layer 5 of the rat visual cortex. III. Differential maturation of axon targeting, dendritic morphology, and electrophysiological properties. *J Comp Neurol* 339: 495–518, 1994c.

Koester SE and O'Leary DD. Functional classes of cortical projection neurons develop dendritic distinctions by class-specific sculpting of an early common pattern. *J Neurosci* 12: 1382–1393, 1992.

Lambolez B, Audinat E, Bochet P, Crepel F, and Rossier J. AMPA receptor subunits expressed by single Purkinje cells. *Neuron* 9: 247–258, 1992.

Larkman A and Mason A. Correlations between morphology and electrophysiology of pyramidal neurons in slices of rat visual cortex. I. Establishment of cell classes. *J Neurosci* 10: 1407–1414, 1990.

Larkum ME, Kaiser KM, and Sakmann B. Calcium electrogenesis in distal apical dendrites of layer 5 pyramidal cells at a critical frequency of back-propagating action potentials. *Proc Natl Acad Sci USA* 96: 14600–14604, 1999a.

Larkum ME, Zhu JJ, and Sakmann B. A new cellular mechanism for coupling inputs arriving at different cortical layers. *Nature* 398: 338–341, 1999b.

Liss B, Franz O, Sewing S, Bruns R, Neuhoff H, and Roeper J. Tuning pacemaker frequency of individual dopaminergic neurons by Kv4.3L and KChip3.1 transcription. *EMBO J* 20: 5715–5724, 2001.

Liss B and Roeper J. Correlating function and gene expression of individual basal ganglia neurons. *Trends Neurosci* 27: 475–481, 2004.

Locke RE and Nerbonne JM. Role of voltage-gated K^+ currents in mediating the regular-spiking phenotype of callosal-projecting rat visual cortical neurons. *J Neurophysiol* 78: 2321–2335, 1997.

Lorincz A, Notomi T, Tamas G, Shigemoto R, and Nusser Z. Polarized and compartment-dependent distribution of HCN1 in pyramidal cell dendrites. *Nat Neurosci* 5: 1185–1193, 2002.

Magee J, Hoffman D, Colbert C, and Johnston D. Electrical and calcium signaling in dendrites of hippocampal pyramidal neurons. *Annu Rev Physiol* 60: 327–346, 1998.

Mahon S, Deniau JM, and Charpier S. Relationship between EEG potentials and intracellular activity of striatal and cortico-striatal neurons: an in vivo study under different anesthetics. *Cereb Cortex* 11: 360–373, 2001.

Mason A and Larkman A. Correlations between morphology and electrophysiology of pyramidal neurons in slices of rat visual cortex. II. Electrophysiology. *J Neurosci* 10: 1415–1428, 1990.

McCormick DA and Prince DA. Post-natal development of electrophysiological properties of rat cerebral cortical pyramidal neurons. *J Physiol* 393: 743–762, 1987.

Paré D, Shink E, Gaudreau H, Destexhe A, and Lang EJ. Impact of spontaneous synaptic activity on the resting properties of cat neocortical pyramidal neurons in vivo. *J Neurophysiol* 79: 1450–1460, 1998.

Ruano D, Lambolez B, Rossier J, Paternain AV, and Lerma J. Kainate receptor subunits expressed in single cultured hippocampal neurons: molecular and functional variants by RNA editing. *Neuron* 14: 1009–1017, 1995.

Schubert D, Staiger JF, Cho N, Kotter R, Zilles K, and Luhmann HJ. Layer-specific intracolumnar and transcolumnar functional connectivity of layer V pyramidal cells in rat barrel cortex. *J Neurosci* 21: 3580–3592, 2001.

Schwindt P and Crill W. Mechanisms underlying burst and regular spiking evoked by dendritic depolarization in layer 5 cortical pyramidal neurons. *J Neurophysiol* 81: 1341–1354, 1999.

Serodio P and Rudy B. Differential expression of Kv4 K^+ channel subunits mediating subthreshold transient K^+ (A-type) currents in rat brain. *J Neurophysiol* 79: 1081–1091, 1998.

Simpson CS, Johnston HM, and Morris BJ. Neuronal expression of protease-nexin 1 mRNA in rat brain. *Neurosci Lett* 170: 286–290, 1994.

Solomon JS, Doyle JF, Burkhalter A, and Nerbonne JM. Differential expression of hyperpolarization-activated currents reveals distinct classes of visual cortical projection neurons. *J Neurosci* 13: 5082–5091, 1993.

Song WJ. Genes responsible for native depolarization-activated K^+ currents in neurons. *Neurosci Res* 42: 7–14, 2002.

Spruston N and Johnston D. Perforated patch-clamp analysis of the passive membrane properties of three classes of hippocampal neurons. *J Neurophysiol* 67: 508–529, 1992.

Steriade M. Neocortical cell classes are flexible entities. *Nat Rev Neurosci* 5: 121–134, 2004.

Steriade M, Timofeev I, Grenier F. Natural waking and sleep states: a view from inside neocortical neurons. *J Neurophysiol* 85: 1969–1985, 2001.

Stewart A and Foehring RC. Calcium currents in retrogradely labeled pyramidal cells from rat sensorimotor cortex. *J Neurophysiol* 83: 2349–2354, 2000.

Stuart GJ and Hausser M. Dendritic coincidence detection of EPSPs and action potentials. *Nat Neurosci* 4: 63–71, 2001.

Turgeon VL, Lloyd ED, Wang S, Festoff BW, and Houenou LJ. Thrombin perturbs neurite outgrowth and induces apoptotic cell death in enriched chick spinal motorneuron cultures through caspase activation. *J Neurosci* 18: 6882–6891, 1998.

Voelker CC, Garin N, Taylor JS, Gahwiler BH, Hornung JP, and Molnar Z. Selective neurofilament (SMI-32, FNP-7 and N200) expression in subpopulations of layer V pyramidal neurons in vivo and in vitro. *Cereb Cortex* 14: 1276–1286, 2004.

Weimann JM, Zhang YA, Levin ME, Devine WP, Brulet P, and McConnell SK. Cortical neurons require Otx1 for the refinement of exuberant axonal projections to subcortical targets. *Neuron* 24: 819–831, 1999.

Williams SR and Stuart GJ. Site independence of EPSP time course is mediated by dendritic I(h) in neocortical pyramidal neurons. *J Neurophysiol* 83: 3177–3182, 2000.

Wise SP and Jones EG. The organization and postnatal development of the commissural projection of the rat somatic sensory cortex. *J Comp Neurol* 168: 313–343, 1976.

Yang CR, Seamans JK, and Gorelova N. Electrophysiological and morphological properties of layers V–VI principal pyramidal cells in rat prefrontal cortex in vitro. *J Neurosci* 16: 1904–1921, 1996.

Zhang ZW. Maturation of layer V pyramidal neurons in the rat prefrontal cortex: intrinsic properties and synaptic function. *J Neurophysiol* 91: 1171–1182, 2004.

Zhu JJ. Maturation of layer 5 neocortical pyramidal neurons: amplifying salient layer 1 and layer 4 inputs by Ca^{2+} action potentials in adult rat tuft dendrites. *J Physiol* 526: 571–587, 2000.